JOURNAL OF SYNCHROTRON RADIATION
ISSN 1600-5775

Performance of photoelectron spin polarimeters with continuous and pulsed sources: from storage rings to free electron lasers

T. Pincelli,[a,b]* F. Grasselli,[c,d] V. N. Petrov,[e] P. Torelli[b] and G. Rossi[a,b]

[a]Dipartimento di Fisica, Università degli studi di Milano, Via Celoria 16, 20133 Milano, Italy, [b]Laboratorio TASC, IOM-CNR, SS 14 km 163.5, Basovizza, 34149 Trieste, Italy, [c]Dipartimento di Scienze Fisiche, Informatiche e Matematiche, Università degli Studi di Modena e Reggio Emilia, Via Campi 213/a, Modena, Italy, [d]S3, Consiglio Nazionale delle Ricerche, Istituto Nanoscienze, Via Campi 213/a, Modena, Italy, and [e]Saint Petersburg State Polytechnical University, Politechnicheskaya Street 29, 195251, Russian Federation. *Correspondence e-mail: pincelli@iom.cnr.it

Received 31 July 2016
Accepted 1 November 2016

Edited by S. Svensson, Uppsala University, Sweden

Keywords: spin-resolved photoemission; spin-polarimetry statistics; intensity fluctuations; pulsed source; continuous source.

In this work the experimental uncertainties concerning electron spin polarization (SP) under various realistic measurement conditions are theoretically derived. The accuracy of the evaluation of the SP of the photoelectron current is analysed as a function of the detector parameters and specifications, as well as of the characteristics of the photoexcitation sources. In particular, the different behaviour of single counter or twin counter detectors when the intensity fluctuations of the source are considered have been addressed, leading to a new definition of the SP detector performance. The widely used parameter called the figure of merit is shown to be inadequate for describing the efficiency of SP polarimeters, especially when they are operated with time-structured excitation sources such as free-electron lasers. Numerical simulations have been performed and yield strong implications in the choice of the detecting instruments in spin-polarization experiments, that are constrained in a limited measurement time. Our results are therefore applied to the characteristics of a wide set of state-of-the-art spectroscopy facilities all over the world, and an efficiency diagram for SP experiments is derived. These results also define new mathematical instruments for handling the correct statistics of SP measurements in the presence of source intensity fluctuations.

1. Introduction

The measurement of spin polarization (SP) of electron beams is a long-standing research programme that has led to the development of advanced instrumentation applied to diverse physical measurements, from nuclear decays to surface spectroscopy and magnetometry. As it is not possible to separate electrons on account of their spin state with the use of Stern–Gerlach apparatus (Kessler, 1985), little efficient spin-dependent scattering effects have to be exploited.

The scattering spin asymmetry can be produced by either exchange interaction between the electrons of the primary beam and the electronic cloud surrounding the target atoms, or by spin–orbit (LS) effects in the deflection electron beam by nuclei of a target. After a long history of developments (Getzlaff *et al.*, 1998; Gay *et al.*, 1992) of spin polarimetry based on LS asymmetry, the present state-of-the-art instruments exploit both kinds of interaction and can be divided into three classes:

(1) *High-energy (0.05–0.5 MeV) LS scattering* (Mott scattering) polarimeters, of which the Compact Classical Mott detector (Petrov *et al.*, 2003) and the Rice-type Mott detector (Burnett *et al.*, 1994) are the most popular designs. These detectors have low values of figure of merit (FOM), due to

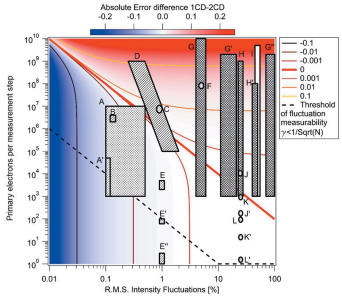

© 2017 International Union of Crystallography

the small elastic back-scattering cross section of high-energy electrons. However, target performance does not degrade on the scale of years, very long integration times are possible, and, if the target is a thin, highly transparent film, the single-scattering approximation allows the polarimeter to be self-calibrating. The asymmetry is measured as an imbalance in the count rate of two electron counters defining specular geometries and operated simultaneously.

(2) *Low-energy LS scattering* (Spin Polarized Low Energy Electron Diffraction; SPLEED), of which the Iridium Spin Filter (Kutnyakhov *et al.*, 2013) is the most recent application. Exploiting the Bragg beam formation in the LEED process, these instruments have higher FOM. They are especially suited for imaging systems, as they allow massive multichannel acquisition. The absence of applied magnetic fields enables spin-filtering to be achieved without perturbing the electron spatial distribution. The target surface can be made stable (Kirschner *et al.*, 2013). The asymmetry signal can be retrieved by combining the images observed at two different scattering electron energies.

(3) *Low-energy exchange scattering* (Very Low Energy Electron Diffraction; VLEED) of which the Fe(001)–p(1×1)O (Bertacco *et al.*, 1998) is now facing a widespread success. These targets have almost two orders of magnitude larger FOM with respect to high-energy LS polarimeters. Thanks to the use of the diffracted (00) beam and the high spin filtering efficiency of exchange scattering, they possess a large statistical advantage over instruments based on different scattering mechanisms. The passivated target has a reasonable stability in ultra-high vacuum (few weeks). The asymmetry is measured by combining subsequent signals recorded with opposite target magnetizations (Okuda *et al.*, 2011).

As SP evaluation is the result of an asymmetry between two values of electron counts (or electron fluxes), a second distinction allows these apparatuses to be further categorized, based on the measurement routine:

(i) *Twin electron counters detectors* (2CDs), illustrated in Fig. 1(*a*), in which the asymmetry is obtained from the difference between two simultaneously measured signals from the electron counters (in the two specular geometries of the scattering events).

(ii) *One electron counter detectors* (1CDs), illustrated in Fig. 1(*b*), in which case asymmetry is evaluated by measuring the signal from a single detector, sequentially changing one of the scattering geometry parameters and measuring again.

Most of the instruments belonging to the low-energy scattering classes (2 and 3) are 1CDs, while those in the high-energy scattering class (1) are mostly 2CDs.

One further dimension to be considered is that each scattering geometry allows for the determination of the spin asymmetry along one of the vector components. If the full SP vector is to be measured then the three components must be obtained. Here it must be noted that two orthogonal components can be simultaneously measured with the high-energy LS Mott polarimeters, using two couples of twin detectors at right angles that are independently but simultaneously sensitive to the two transverse spin polarization components of the incoming electron beam. The same result for a 1CD polarimeter requires four subsequent measures each with a geometry determined by the scattering sample magnetization that must be set in the four directions along the two perpendicular quantization axes.

As the new generation of extremely brilliant coherent and ultra-short pulsed sources are coming on-line [free-electron lasers, or FELs (Galayda *et al.*, 2010; Hara *et al.*, 2012; Amann *et al.*, 2012; Allaria *et al.*, 2012, 2013; Ayvazyan *et al.*, 2006), ultraviolet solid-state lasers, gas generation of high harmonics, or HHGs (Lorek *et al.*, 2014; Leitner *et al.*, 2011)], new photoemission techniques can be developed with access to different regimes of excitation and pump–probe protocols. Applications to high-resolution measurements allowing for the simultaneous measurement of energy, momentum and spin polarization as in angle-resolved photoemission spectroscopy (ARPES) experiments (Dil, 2009; Hoesch *et al.*, 2002) have developed recently enhancing substantially the efficiency of spin-ARPES (Das *et al.*, 2016; Suzuki *et al.*, 2014; Okuda *et al.*, 2011; Bigi, 2016) and, in fact, making high-resolution 'complete photoemission experiments' possible (Schönhense *et al.*, 2015).

Understanding the optimal experimental approach to the SP measures in these novel experiments is of primary importance, both for the best exploitation of the scarce beam-time at FELs/X-FELs and for the best statistical value of the data.

The performance of a spin detector is classically evaluated by trying to achieve the highest Shermann function [for formal definition see §2, equation (1)] and the highest FOM [for a formal definition see §2, equation (4)]. The aim of this work is to show that, in the present complex panorama of different applications, these two parameters might be misleading, and a full statistical analysis, accounting for the whole process behind the electron spin polarization measurement, is necessary to identify the most performing instrument for a certain application. We carried out such evaluation with particular attention to the statistics of electron spin polarization measurements accounting for the intensity fluctuations of the sources. This enables us to identify the various regimes in which each kind of instrument is best performing, and to lay down a map of the ranges of applicability.

2. Spin–orbit-based detectors

Spin–orbit-based apparatuses retrieve asymmetry from the process known as Mott scattering (Mott, 1929, 1932), studied by Sir N. Mott in 1929. When an incoherent beam of high-energy electrons (0.05–0.5 MeV) impinges on a heavy-atom target, it is diffused incoherently in every direction of space, mostly due to the charge (Coulomb) scattering. A spin–orbit (LS) component of the scattering potential is nevertheless present as, in the frame of the electron, the target nuclei are seen as rotating charges during the scattering deflection, and the sense of rotation depends on the approaching trajectory of the electron with respect to the fixed nuclei in the crystal (and laboratory) frame. The relative amplitude of the LS scattering potential (anisotropic) with respect to the Coulomb potential

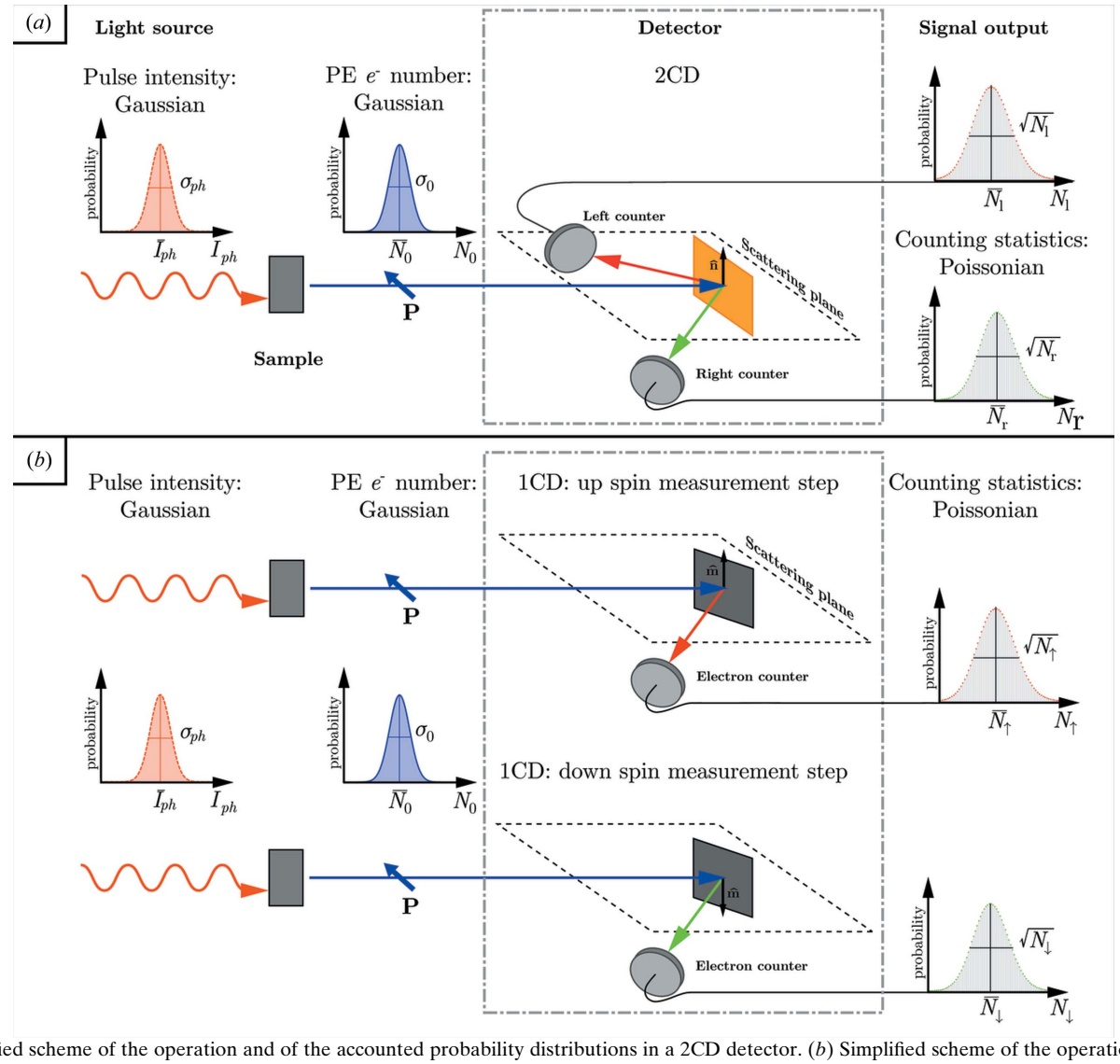

Figure 1
(*a*) Simplified scheme of the operation and of the accounted probability distributions in a 2CD detector. (*b*) Simplified scheme of the operation and of the accounted probability distributions in a 1CD detector. It is divided into two subfigures in which the two successive steps needed for a single polarization measurement are shown.

(isotropic) depends strongly on the final deflection angle for the elastically scattered electrons. At small deflection angles the LS effect is negligible and non-measurable, but at some large angles it becomes relevant. It has been demonstrated that for deflection angles of 120° the LS effect on the total scattering cross section is relatively large and measurable: it is then possible to determine a geometry-dependent asymmetry that corresponds to a SP asymmetry of the primary beam in the direction perpendicular to the scattering plane, defined by the beam itself and the detector position in the laboratory frame. If the primary beam has a polarization vector **P**[1], the differential cross section at angle θ is given by

$$\left(\frac{\mathrm{d}\sigma}{\mathrm{d}\Omega}\right)_{\mathrm{SL}} = I(\theta)[1 + S(\theta)\,\mathbf{P}\cdot\hat{\mathbf{n}}], \tag{1}$$

where

(i) $I(\theta)$ is the spin-averaged cross section, cancelling out the effects of spin.

(ii) $S(\theta)$ is a function, called the *Sherman function* (Sherman, 1956), dependent on the angle of deflection, that expresses the efficiency with which the scattering process selects the spin.

(iii) $\hat{\mathbf{n}}$ is the quantization axis unit vector.

If a partially polarized beam (with non-vanishing components of **P** in the direction of $\hat{\mathbf{n}}$) impinges with an energy in the proper range on a heavy-atom target, then the number of electrons scattered on the right $[N(\theta) = N_{\mathrm{r}}]$ and on the left $[N(-\theta) = N_{\mathrm{l}}]$ will be different, and the *asymmetry function* can be defined:

[1] The polarization vector **P** of an ensemble of electrons is defined as $\mathbf{P} = \sum_n \langle\varphi^{(n)}|\boldsymbol{\sigma}|\varphi^{(n)}\rangle \,/\, \sum_n \langle\varphi^{(n)}|\varphi^{(n)}\rangle$, where $|\varphi^{(n)}\rangle$ are the pure spin states and $\boldsymbol{\sigma}$ is the Pauli operator, *i.e.* a three-component vector of Pauli matrices. It is, therefore, along any spatial direction, the ensemble-averaged expectation value of the spin operator. Its modulus is therefore always between 0 (completely unpolarized beam) and 1 (beam completely polarized along one direction).

$$A(\theta) = \frac{N_r - N_l}{N_l + N_r}. \quad (2)$$

Therefore, by measuring $A(\theta)$, it is possible to evaluate the normal component to the scattering plane of the spin-polarization vector of the primary beam:

$$P = \frac{1}{S(\theta)} A(\theta). \quad (3)$$

This is the basic operational principle of the Mott polarimeter (Kessler, 1985), that withstood a long process of evolution and refinement from the first prototypes (Shull *et al.*, 1943) to the present advanced instruments (Petrov *et al.*, 2007; Pincelli *et al.*, 2016; Strocov *et al.*, 2015). It is crucial to note, in the light of the following discussion, that these polarimeters intrinsically allow for the use of two electron counters operated simultaneously at opposing angles. In fact, the geometry asymmetry (left–right) corresponding to the LS extra deflection can be exploited directly. A one-dimensional Mott scattering experiment can certainly be carried out, by measuring subsequent intensities for electron beams of reversed SP, but it is certainly not the efficient way to go!

In fact, even four detectors can be operated in a Mott polarimeter as both the transversal components of the SP of the electron beam can be simultaneously determined along two mutually perpendicular scattering planes, both containing the electron beam.

It must be appreciated that a scattering angle of 120° is quite unfavourable at these energies (single-scattering regime, thin target film to avoid multiple scattering) and that consequently the overall counting statistics are low.

When comparing different kinds of polarimeters, it is customary to use a quantity called the *figure of merit*. It roughly quantifies the performance of a spin detector, and is defined as

$$\varepsilon = \left(\frac{N_r + N_l}{N_0}\right) S_{\rm eff}^2, \quad (4)$$

where N_0 is the beam intensity entering the polarimeter, $N_l + N_r$ is the total scattered intensity measured by the detectors and $S_{\rm eff}$ is the effective Sherman function[2] of the detector. As will be discussed below, state-of-the-art Mott polarimeters based on high-energy spin orbit scattering can achieve $\varepsilon = 6 \times 10^{-4}$, mainly due to the low value of the ratio $(N_r + N_l)/N_0$: the cross section of such large angle deflections required to efficiently select spin is rather low.

Lower-energy apparatuses based on spin–orbit effects have also been built, both as 2CD (Yu *et al.*, 2007) and as 1CD (Tusche *et al.*, 2013; Kutnyakhov *et al.*, 2013; Kirschner *et al.*, 2013). From the purely theoretical point of view, low-energy 2CD systems can be described with the same equations (1), (2) and (3), obviously with a different effective $S(\theta)$ as the multiple scattering dominates at low electron energies and $S(\theta)$ cannot be calculated simply as in the case of single scattering. The low-energy 1CD systems, recently developed, require that the energy of the primary beam is modified to evaluate the asymmetry: the discussion of the performance of these systems can be developed along the same lines of that for exchange-based detectors, described below.

[2] While the Sherman function is calculated for an ideal, single-atom scattering experiment, in a real detector other factors can arise that further reduce the efficiency of spin selection: contamination of the target, multiple elastic scattering, finite angular acceptance of the detectors. Furthermore, the scattering angle and energy are fixed to the values that maximize the asymmetry. The effective Sherman function will therefore be a *number* obtained by a calibration measurement, accounting for all such different effects.

3. Exchange-based detectors

As the energy of the primary beam is lowered enough, the electrons interact in the full multiple scattering regime with the detailed electronic structure of the solid. Exchange effects take the dominant role in determining the SP-dependent amplitudes. These experiments require the use of thin films of 3*d* ferromagnets as a target, possessing a reduced spin–orbit scattering contribution but a large exchange splitting of the electronic states. The quantization axis is now given by the magnetization direction of the target, which defines the component of the polarization vector that is probed. In particular, Bertacco & Ciccacci (1999) demonstrated that the exchange-split band-gap in the empty states (6 eV above E_f) of the Fe–O(1×1)p passivated surface gives a very strong asymmetry both in reflection and adsorption when a polarized beam impinges on it. Building the formalism in analogy with equation (1):

$$\left(\frac{d\sigma}{d\Omega}\right)_{\rm ex} = I(\theta)\left[1 + S^{(\rm ex)}(\theta)\, \mathbf{P} \cdot \hat{\mathbf{m}}\right], \quad (5)$$

where $\hat{\mathbf{m}}$ is a unit vector representing the direction of the target's magnetization. When building the normalized asymmetry [as in equation (2)], however, the radical difference between the two approaches sets in. Having lost the LS dominant effect, the geometrical asymmetry is lost and with it the possibility of measuring simultaneously the right–left asymmetry, *i.e.* to perform two specular experiments with two detectors per scattering plane. Exchange-based detectors require that an intensity measurement is performed with magnetization in the 'up' direction ($N_\uparrow$), then magnetization is reversed in the 'down' direction, and a second acquisition ($N_\downarrow$) is made. These two can be combined to give a *single evaluation* of asymmetry:

$$A_{\rm ex} = \frac{N_\uparrow - N_\downarrow}{N_\uparrow + N_\downarrow}. \quad (6)$$

Through the cross section in equation (5) it is then possible to find

$$P_{\rm m} = \frac{1}{S_{\rm eff}^{(\rm ex)}} A_{\rm ex}, \quad (7)$$

where $P_{\rm m}$ is the component of polarization in the magnetization direction and $S_{\rm eff}^{(\rm ex)}$ represents the effective Shermann function of the system.

It is now clear that, requiring two separated measurements and an energy so low (6 eV) that only the (00) beam of LEED pattern appears, exchange-interaction-based apparatuses are intrinsically 1CD. These systems were developed in the quest for higher efficiencies with continuous and stable sources, and they actually represent an extraordinary advancement [$\varepsilon \simeq 10^{-2}$ have been reached (Graf *et al.*, 2005)].

4. Error in polarization measurement

In order to discuss the topic more clearly, it is better to introduce the basic formulas by deriving them under the assumption of a non-fluctuating stationary electron current. This will also enable us to show the conceptual pattern that is repeated in the following steps, when coping with the more complicated temporal fluctuation regime.

The uncertainty on polarization defined in equation (3) can be evaluated, using the propagation for independent errors, as

$$\Delta P = P\left[\left(\frac{\Delta A}{A}\right)^2 + \left(\frac{\Delta S_{\rm eff}}{S_{\rm eff}}\right)^2\right]^{1/2}. \tag{8}$$

ΔP has two sources: a statistical one (related to ΔA) and a systematic one (caused by $\Delta S_{\rm eff}$). The systematic error is reduced during the calibration of the detector, when $S_{\rm eff}$ is measured as accurately as possible. However, it is very difficult to realise accurate measurements because of the intrinsic low statistics of both methods of calibration.[3] Once $\Delta S_{\rm eff}$ is determined, it cannot be changed and does not affect significantly the measurement routine, as substitution of typical values shows that even a 10% uncertainty on $S_{\rm eff}$ does not contribute significantly to ΔP. As it is irrelevant to our discussion, in the following it will be neglected. The only uncertainty on P is therefore assumed to be due only to statistical counting errors in ΔA.

The relative error $\delta A = \Delta A/A$ can be calculated as [see equation (2)]

$$\delta A = \left[\left(\frac{\Delta{\rm Diff}}{N_{\rm r} - N_{\rm l}}\right)^2 + \left(\frac{\Delta{\rm Sum}}{N_{\rm r} + N_{\rm l}}\right)^2\right]^{1/2} \tag{9}$$

where ΔDiff (ΔSum) is the absolute error on $N_{\rm r} - N_{\rm l}$ ($N_{\rm r} + N_{\rm l}$). It follows that ΔDiff = ΔSum. The second summand can be neglected, as it is much smaller than the first,

$$\delta A \simeq \left[\left(\frac{\Delta{\rm Diff}}{N_{\rm r} - N_{\rm l}}\right)^2\right]^{1/2} \equiv \left[\frac{(\Delta N_{\rm l})^2 + (\Delta N_{\rm r})^2}{(N_{\rm r} - N_{\rm l})^2}\right]^{1/2}. \tag{10}$$

Assuming that the variances for $N_{\rm r}$ and $N_{\rm l}$ are determined by two independent Poissonians[4] and

$$\Delta A = \delta A \cdot A = \frac{1}{(N_{\rm l} + N_{\rm r})^{1/2}}, \tag{11}$$

and, dividing by $S_{\rm eff}$ to obtain polarization uncertainty,

$$\Delta P = \left[\frac{1}{(N_{\rm r} + N_{\rm l})S_{\rm eff}^2}\right]^{1/2}. \tag{12}$$

Now, introducing N_0 as defined in equation (4), it is possible to write

$$\varepsilon = \left(\frac{I}{I_0}\right)S_{\rm eff}^2 = \left(\frac{N_{\rm r} + N_{\rm l}}{N_0}\right)S_{\rm eff}^2. \tag{13}$$

Finally, one has,

$$\Delta P = \frac{1}{(N_0\varepsilon)^{1/2}}. \tag{14}$$

For this reason the FOM has been regarded as a fundamental parameter of SP experimental apparatuses until now. However, as will be shown in the following, the advent of pulsed sources with strong intensity fluctuations is dramatically changing the experimental conditions, reducing the importance of such a parameter and shifting the focus towards set-ups able to reject the source intensity noise.

5. Absolute error in the presence of intensity fluctuations

As discussed above, a measurement of electron beam SP by necessity consists of a difference between two measured intensities. The electrons are always counted in a finite, discrete time, that we will call a 'measurement step': either the integration time window (with a continuous or quasi-continuous source) or the duration of the bunch generated by a single excitation pulse as it is the case with the novel short-pulsed sources. In both cases, the intensity fluctuations of the source, although on very different time-scales, must be thoroughly accounted to understand their role in the statistics of the polarization measurement. In the following, the intensity fluctuations will be discussed in general. At the end of each section, the discussion will be exemplified for the case of measurement of the spin polarization of the secondary electrons, in an experiment in which separate, high-intensity shots from a FEL are measured. This case represents the limit case, in which fluctuations are extremely large, while the intensity is extremely high. This is the region in the parameter space that yields the most counter-intuitive results. At the end of the section, the whole parameter space will be addressed. The discussion (bearing no constraints on the actual timescale of the measurement step) can therefore be adapted to all kinds of sources.

In the following discussion we will assume that the electron detectors and counters of the polarimeter are able to handle the electron bunches scattered off the target surface without saturating. As the number of electrons reaching the detector can have very high peak currents (up to 10^{12} electrons s^{-1}, corresponding to a bunch of 10^5 electrons spread over about 100 ns), this is not an obvious task. Very recently, however, it has been demonstrated in a state-of-the-art Mott polarimeter set-up (Pincelli *et al.*, 2016), so we considered it a solvable experimental problem and we neglected it.

[3] The first method is *double scattering* (Kessler, 1985). The second method is called *energy acceptance reduction* (Gay & Dunning, 1992).
[4] This is true since the signals are retrieved from two independent detectors.

5.1. Fluctuations for 2CD

The number of primary electrons is now defined by the measurement step

$$N_0 = N_0(i), \tag{15}$$

where $N_0(i)$ is the number of electrons entering the detector during the ith measurement step. It is possible[5] to assume that this is proportional to the intensity of the light during the ith measurement step. The intensity distribution is generally described by a Gaussian with finite variance.

If a 2CD is considered, it is possible to treat the single measurement step in the same way as was done for a continuous flux of electrons. By simple substitution of N_0 in equation (14), we obtain

$$\Delta P(i) = \frac{1}{\left[N_0(i)\varepsilon\right]^{1/2}}. \tag{16}$$

Performing a weighted average over n_p measurement steps, the uncertainty reads:

$$\Delta P(n_\mathrm{p}) = \frac{1}{\left[\sum_{i=1}^{n_\mathrm{p}} 1/\Delta P(i)^2\right]^{1/2}} = \frac{1}{\left[\sum_{i=1}^{n_\mathrm{p}} N_0(i)\varepsilon\right]^{1/2}}. \tag{17}$$

This procedure is thus very efficient in handling the instabilities of the source, because the weighted average enables taking little account of polarization measurements coming from very low intensity measurements that carry a very high uncertainty.

If one assumes to know the average number of electrons per measurement step, N_epp, it is possible to consider n_p so big that

$$\sum_{i=1}^{n_\mathrm{p}} N_0(i) = n_\mathrm{p}\bar{N}_\mathrm{epp} \tag{18}$$

and to consider the asymptotic behaviour

$$\Delta P(n_\mathrm{p}) \simeq \left(\frac{1}{n_\mathrm{p}\bar{N}_\mathrm{epp}\varepsilon}\right)^{1/2}. \tag{19}$$

The uncertainty thus scales as the square root of $1/n_p$.

If we include the typical values of measurement of the spin polarization of the secondary electrons (*e.g.* Petrov & Kamochkin, 2004; Fognini *et al.*, 2014), $\varepsilon \simeq 6 \times 10^{-4}$ and $\bar{N}_\mathrm{epp} \simeq 10^5$, we obtain

$$\Delta P(n_\mathrm{p}) \simeq 0.129/\sqrt{n_\mathrm{p}}. \tag{20}$$

5.2. Fluctuations for 1CD

The asymmetry for a 1CD polarimeter was given in equation (6) but a subtle point must be considered when passing to the fluctuation regime. If the intensity counted in each measurement step was constant and equal to $\mathcal{N}_0$, the asymmetry that one would expect to measure is:

$$A^\mathrm{th} = \frac{\mathcal{N}_0\sigma_\uparrow - \mathcal{N}_0\sigma_\downarrow}{\mathcal{N}_0\sigma_\uparrow + \mathcal{N}_0\sigma_\downarrow}, \tag{21}$$

where $\sigma_\uparrow$ and $\sigma_\downarrow$ are the cross sections for electrons with opposite spin state. In the real measurement, however, the electrons for $\sigma_\uparrow$ and $\sigma_\downarrow$ are subject to changes due to source fluctuations, and their number is different. It is then necessary to write

$$A^\mathrm{real}(i, i+1) = \frac{N_\uparrow(i) - N_\downarrow(i+1)}{N_\uparrow(i) + N_\downarrow(i+1)}. \tag{22}$$

Each of the measurements of $N_{\uparrow(\downarrow)}$ will be affected by the usual counting statistics of the electron counters so that:

$$N_\uparrow(i) = N_0(i)\sigma_\uparrow \pm \Delta N_{\uparrow\mathrm{stat}}(i) \tag{23}$$

and

$$N_\downarrow(i+1) = N_0(i+1)\sigma_\downarrow \pm \Delta N_{\downarrow\mathrm{stat}}(i+1). \tag{24}$$

If one wants to refer to the expected asymmetry, however, one must introduce a third error 'pairwise' ΔN_pp when computing the numerator and denominator, due to the fact that intensity fluctuations exist from one measurement step to the next.[6] It is then possible to calculate the relative uncertainty:

$$\delta A(i, i+1) = \left[\frac{\Delta N^2_{\uparrow\mathrm{stat}}(i) + \Delta N^2_{\downarrow\mathrm{stat}}(i+1)}{\left[N_\uparrow(i) - N_\downarrow(i+1)\right]^2} + \frac{\Delta N^2_\mathrm{pp}(i, i+1)}{\left[N_\uparrow(i) - N_\downarrow(i+1)\right]^2}\right]^{1/2},$$

where $[\Delta N^2_{\uparrow\mathrm{stat}}(i) + \Delta N^2_{\downarrow\mathrm{stat}}(i+1)]$ is the absolute error on the numerator of A and the relative errors concerning the denominator have been neglected. Considering Poisson statistics for the counting errors, it is now possible to obtain the absolute error on asymmetry and, dividing by the effective Shermann function S_eff, the absolute error on polarization,

$$\Delta P(i, i+1) = \frac{1}{S_\mathrm{eff}\left[N_\uparrow(i) + N_\downarrow(i+1)\right]^{1/2}} \times \left[1 + \frac{\Delta N^2_\mathrm{pp}}{N_\uparrow(i) + N_\downarrow(i+1)}\right]^{1/2}. \tag{25}$$

It is then evident that an object very close to the uncertainty observed in 2CDs is obtained by multiplication of the prefactor with the first summand under the square root. A second term, arising from the instability of the source, is now present and increases the error as there are only non-negative numbers.

[5] The effects of space charge, that distort the proportionality between light intensity and electron yield (Fognini *et al.*, 2014), are neglected here.

[6] It must be noted that the errors are of a statistical nature. Despite the fact that now ΔN_pp is introduced as a difference between two precise measurement steps, if one wants to deal with it as an error on the intensity measurement one must consider ΔN_pp as the variance of the distribution of the differences, just as one uses the variance of the Poissonian distribution centred at $N_\uparrow(i)$ for $\Delta N_{\uparrow\mathrm{stat}}(i)$ or at $N_\downarrow(i+1)$ for $\Delta N_{\downarrow\mathrm{stat}}(i+1)$.

If several measurements are performed, a weighted average can be used again, yielding

$$\Delta P(n_{\rm p}) = 1 \Big/ \left\{ \sum_{i=1}^{n_{\rm p}} \frac{S_{\rm eff}^2 \left[N_\uparrow(i) + N_\downarrow(i+1)\right]^2}{N_\uparrow(i) + N_\downarrow(i+1) + \Delta N_{\rm pp}^2} \, \delta_{(i \bmod 2,1)} \right\}^{1/2}, \tag{26}$$

where $\delta_{(i \bmod 2,1)}$ is the Kronecker Delta and mod is the modulo function, allowing to keep only the odd values of i. This is because each *asymmetry value* is now obtained only after *two measurement steps*. Stepping again to the limit of large $n_{\rm p}$ it is possible to consider:

$$S_{\rm eff}^2 [N_\uparrow(i) + N_\downarrow(i+1)] \simeq S_{\rm eff}^2 (\bar{N}_\uparrow + \bar{N}_\downarrow) = 2\bar{N}_0 \, \varepsilon. \tag{27}$$

The sum results in a simple multiplication by the number of observed asymmetry values, *i.e.* $n_{\rm p}/2$, giving

$$\Delta P(n_{\rm p}) = \left[\frac{1}{n_{\rm p} \bar{N}_0 \varepsilon} \left(1 + \frac{\Delta N_{\rm pp}^2}{\bar{N}_\uparrow + \bar{N}_\downarrow} \right) \right]^{1/2}, \tag{28}$$

where $\bar{N}_\uparrow$ and $\bar{N}_\downarrow$ are the average intensities measured in the two magnetization configurations, $\bar{N}_0$ is the average number of electrons per measurement step before the polarimeter, and ε is the FOM of the detector given in equation (4), substituting $N_{\rm r(l)}$ with $\bar{N}_{\uparrow(\downarrow)}$.

To evaluate $\Delta N_{\rm pp}$ the discussion needs to be deepened slightly further. This uncertainty is generated by the fact that $N_0(i)$ and $N_0(i+1)$ are two successively and independently extracted variables from the same normal distribution:

$$\mathcal{P}\left[N_0(i)\right] = \frac{1}{\left(2\pi\sigma_0^2\right)^{1/2}} \exp\left\{ -\frac{\left[N_0(i) - \bar{N}_0\right]^2}{2\sigma_0^2} \right\}, \tag{29}$$

where σ_0 is the variance in the distribution of number of primary electrons. This quantity can be traced back to the relative variance $\gamma \equiv \sigma_{\rm ph}/\bar{I}_{\rm ph} = \sigma_0/\bar{N}_0$ in the photon beam intensity on the appropriate time-scale, *i.e.* the same as the measurement step. The latter equality comes from the relationship between intensity and number of photoemitted electrons that is supposed to be linear in this range. $\Delta N_{\rm pp}$ can therefore be calculated by Gaussian integration (see Appendix *A*), giving

$$\Delta N_{\rm pp} \simeq \frac{1}{\sqrt{2}} \left(\bar{N}_\uparrow + \bar{N}_\downarrow\right)\gamma \approx \frac{\sqrt{2}\,\bar{N}_0 \, \varepsilon}{S_{\rm eff}^2} \, \gamma, \tag{30}$$

where the last approximation comes from equation (27). Substituting in equation (28) we obtain

$$\Delta P(n_{\rm p}) \simeq \left[\frac{1}{n_{\rm p}} \left(\frac{1}{\bar{N}_0 \, \varepsilon} + \frac{\gamma^2}{S_{\rm eff}^2} \right) \right]^{1/2}. \tag{31}$$

In the regime of large $\bar{N}_0$, the first summand of the factor in square parenthesis is much smaller than the other. It is then possible to write

$$\Delta P(n_{\rm p}) \simeq \left(\frac{1}{n_{\rm p}} \right)^{1/2} \frac{\gamma}{S_{\rm eff}}. \tag{32}$$

Applying again to the case of the spin-polarization of the secondary electrons with the FEL source, we can substitute[7] $S_{\rm eff} \simeq 0.35$ (Okuda *et al.*, 2011), $\bar{N}_0 \simeq 10^5 \gamma \simeq 0.1$ then one obtains

$$\Delta P(n_{\rm p}) \simeq 0.286 / \sqrt{n_{\rm p}}, \tag{33}$$

i.e. despite the lower FOM, the 2CDs have a coefficient a factor of three smaller. This means that a repetition rate nine times smaller is required to perform experiments with the same precision and the same duration, or that nine times shorter experiments are required for 2CDs at the same repetition rate. It is interesting to observe that, in the parameter configuration used in this example, the coefficient of the 1CD is strongly dependent on γ, and only weakly on $\bar{N}_0$ [equation (31)], while for the 2CD the situation is exactly the opposite: the coefficient is determined mainly by $\bar{N}_0$ and has no dependence on γ.

Our derivation therefore allows us to individuate some regimes in which the advantage of monitoring the intensity given by 2CDs results in shorter measurements despite the higher efficiency attainable with 1CDs. In Fig. 2 (see also Table 1), a density plot of the difference between the absolute error values of 1CDs and 2CDs ($\Delta P_{\rm 1CD} - \Delta P_{\rm 2CD}$), averaged over 100 measurement steps, is plotted *versus* the number of electrons entering the detector per measurement step and of the intensity fluctuations of the source.

As our paper aims at mapping out the regimes (and consequently the category of light sources) with which the measurement mechanism of every spin detector is most efficiently used, we overlaid to the density plot a scheme depicting the regime of operation of state-of-the-art light sources.

As explained in §5, it is also possible to account for intensity fluctuations also for continuous sources. If the r.m.s. fluctuations are evaluated in the same time window as the integration time of the electron counters, the statistical treatment of both 1CD and 2CD errors is identical to the one followed above. For this reason, continuous and quasi-continuous sources have been added to Fig. 2. For continuous sources, the time duration of a measurement step was arbitrarily set at 1 s, and correspondingly the r.m.s. intensity fluctuations on 1 s gating time were used.

Estimate of photoemission experiment intensities have been obtained:

(i) by using measured data when available;

(ii) by multiplying the photon flux and its r.m.s. fluctuations, assuming

(*a*) quantum efficiency (QE) of a gold surface, 10^{-1} @ 30 eV, 10^{-3} @ 6–7 eV,

(*b*) 10^{-3} in the case of direct transport to the spin detector, 10^{-5} for detection after the energy analyzer.

[7] It should be noted that $\gamma \simeq 0.1$ is a rather generous estimate, based on the reported (Hara *et al.*, 2012) performance of SACLA FEL in Japan. Most FELS operate with higher shot-to-shot fluctuations.

Table 1
References of the symbols shown in Fig. 2.

Symbol	Reference	Symbol	Reference
A, A′	A†	G′	Hara *et al.* (2012)
B	Okuda *et al.* (2011)	G″	Amann *et al.* (2012)
C	Shimojima *et al.* (2015)	H	Allaria *et al.* (2012)
D	D‡	H′	Allaria *et al.* (2013)
E	Bergeard *et al.* (2011)	I	Ayvazyan *et al.* (2006)
E′, E″	Holldack *et al.* (2014)	J, K, J′, K′	Lorek *et al.* (2014)
F	F§	L, L′	Leitner *et al.* (2011)
G	Galayda *et al.* (2010)		

† Obtained from a survey on the declared photon flux values of a large number of photoemission beamlines as made possible by websites of coordinated access projects such as http://wayforlight.eu/eng/search-beamlines.aspx. Measurements performed by the authors on APE-LE beamline (A′) confirm part of this range. ‡ As obtained with a commercial e-gun on measurements performed by the authors. § From typical performance of a high-intensity femtosecond Ti:Sa laser combined with a 10% efficiency 4HG stage.

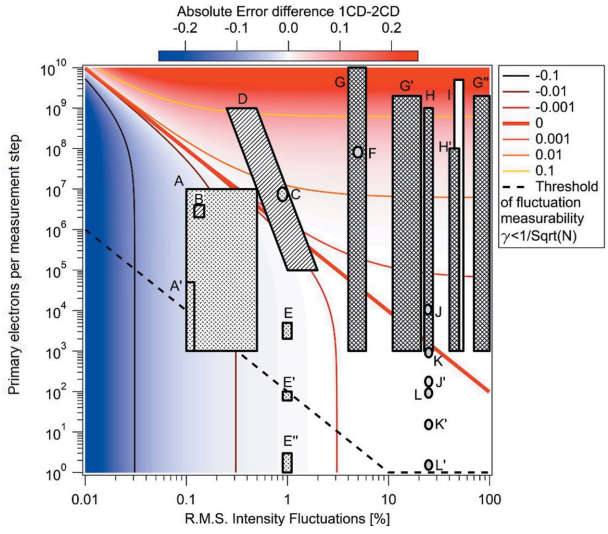

Figure 2
Expected range of application with different sources. The dotted mesh (A, A′, C, E, E′, E″) defines quasi-continuous sources, the continuous-line mesh defines continuous sources (B, D), the light gray mesh defines pulsed solid-state lasers (F, J, J′, K, K′, L, L′), the rhombohedral mesh 'hot' FELs (G, G′, G″, H, H′) and the white fill indicates superconducting FELs (I). A, A′: synchrotron beamline. B: helium lamp. C: quasi-CW VUV laser. D: electron gun. E′, E″: femtoslicing synchrotron beamline. F: table-top laser 4HG. G: LCLS hard-X FEL. G′: SACLA hard-XFEL. G″: LCLS self-seeding. H: Fermi FEL-1 (seeded). H′: Fermi FEL-2 (seeded, cascaded). I: FLASH FEL (SASE). J, K, J′, K′: high-power HHG laser (fluctuations inferred from L). L, L′: mid-power HHG laser (for which shot-to-shot fluctuations were accurately measured).

Considering the following issues as solvable by adapting the individual apparatus to the effective mode of operation, we have ignored the following:

(i) space charge effects,

(ii) fine details of electrostatic lenses transmittance,

(iii) the possibility of saturation of electron counters,

(iv) sample degradation effects or disruption by Coulomb explosion.

Care must be taken in reading this diagram, as the effective time required for an experiment is also defined by the repetition rate of the source, which is somehow hindered by the normalization to the number of measurement steps used here: J operates at 20 kHz for example, while G at 10 Hz. The detailed source parameters are listed in Appendix *B*.

Fig. 2 also shows (as a dashed black line) the threshold below which the intensity fluctuations are not measurable, as they are smaller than the counting statistics for each pulse (or second):

$$\gamma = 1/\sqrt{N}. \tag{34}$$

For values of γ smaller than $1/\sqrt{N}$, the amount of electrons in each pulse is large enough to make the Poisson uncertainty on counting statistics dominating over the intensity fluctuation noise.

We have demonstrated that, in general, the difference between the 2CDs and 1CDs grows in favour of the former if the average number of electrons per measurement step grows, when combined with a large instability of the source. This points at a more efficient application of 2CDs with FELs, whose emission has matching characteristics. However, several hurdles stand before the application of photoemission techniques with the full photon flux of a FEL source.

The most relevant is the space charge effect. For most of the photoelectron spectroscopies (especially ARPES), the present limit for spin-integrated measurements is of one electron per pulse per reasonable energy and angle interval. Above this, the spectra suffer reduced resolution and deformations. In this configuration, the statistics for single-shot spin polarization measurements are insufficient for both machines, and several shots have to be counted, making the experiment barely feasible at the typical repetition rates of a FEL.

However, very recent experiments of measurement of the spin polarization of the secondary electrons (Fognini *et al.*, 2014) have demonstrated the feasibility of experiments with more than 10^6 electrons per pulse, although with reduced polarization signal. The compromise between reduction of the signal and reduction of the uncertainty will probably have to be addressed practically, depending on the aim of the experiment.

On the other hand, the higher FOM of the 1CDs allows them to outperform significantly the 2CDs when lower intensity but higher stability sources are considered. ARPES is therefore more immediately applied to this configuration, and this has already been done (Okuda *et al.*, 2011; Bigi, 2016). Yet, also these configurations are extremely photon-hungry, and the ARPES community would surely benefit if the full potential of FEL brilliance was to be unlocked. There is therefore an on-going effort in trying to overcome this issue that has been addressed by Hellmann *et al.* (2009), Schönhense *et al.* (2015) and Verna *et al.* (2016).

Nonetheless, our statistical framework will have to be addressed every time one uses a source of intensity sufficient to achieve $\gamma > 1/\sqrt{N}$, independently of how the issue of space charge is addressed, may it be with strong accelerating fields close to the sample (Schönhense *et al.*, 2015), *a posteriori* data treatment (Schönhense *et al.*, 2015; Dell'Angela *et al.*, 2015) or exploiting complex time-structures of the pulsed beam (Hellmann *et al.*, 2012). The method is also applicable to any kind of spin-resolved photoelectron spectroscopy from

energy-integrated measurement of the polarization of the secondary electron yield to the single-channel spin-ARPES, and even to the parallel acquisition spin-ARPES that is now being addressed in different ways (Schönhense *et al.*, 2015; Strocov *et al.*, 2015), as only the number of electrons entering the polarimeter is relevant for the discussion.

When the vectorial determination of SP is sought, the above analysis has to be applied to the three components of SP. Here the 2CDs are 'upgraded' easily to four-channel detectors (4CDs) allowing the same measurement time to provide both the transversal components of SP of the analysed electron beam. Only the third component requires a subsequent measurement act. In the case of Mott polarimeters this can be performed either by alternatively addressing two identical but orthogonal polarimeters by deviating electrostatically the electron beam every other pulse to one or the other of the polarimeters, or by 'rotating' the SP of the incoming beam by a magnetic rotator and observing the scattering in the same polarimeter. Also when using 1CD exchange polarimeters two orthogonal apparatuses are needed and a sequence of several measurements steps are required. The minimum number is six, in order to measure the three components of the polarization vector. In case cross-confrontation of the two independent apparatuses is necessary, the four magnetization orientations of each of two targets have to be measured, giving eight separate measurement steps for a single evaluation of the spin polarization vector. In this case an internal calibration can be exploited as one SP component is measured twice (once in each polarimeter). Therefore, the measurement of the spin polarization vector will require at least two separate measurement steps to a 4CD, while at least six measurement steps to a 1CD. Besides the factor of three in the number of measurement steps, γ will appear once for each component in the 1CD, as the measurement steps are all temporally interdependent in pairs. In the 4CD, instead, γ will never appear, as the measurement steps are all temporally independent of each other.

6. Numerical experiments

Numerical experiments have been performed in order to simulate the two considered experimental setups of the measurements, *i.e.* the 2CD and the 1CD apparatuses, and to perform a statistically reliable set of simulations to validate the theoretical results discussed above. The numerical code has been written in Mathematica programming language. We sketch, for clarity, a list of the main sets of operations adopted in the numerical simulation plan, in which we tried to follow the true experimental procedure.

The simulation of experiments with 2CD detectors was developed in the following steps:

(i) We imagined the *true* polarization of the electron beam, photoemitted from the sample, $P^{\rm true}$, to be *fixed*, since it is an intrinsic property of the physical system.

(ii) We fixed the known physical parameters of the apparatus, *i.e.* $\bar{N}_0$, $S_{\rm eff}$, σ_0, $\varepsilon_{\rm 2CD(1CD)}$.

(iii) We started a loop over the number of measurement steps, i, from 1 to a certain maximum value $n_{\rm p}^{\rm max}$, in which, for each iteration:

(a) We *randomly* extracted with Gaussian probability, representing the distribution of the number of photoemitted electrons (centred in $\bar{N}_0$, and with a standard deviation of σ_0), the specific number of photoemitted electrons of the ith iteration, $N_0(i)$.

(b) From $N_0(i)$ we calculated the two quantities

$$N^0_{\rm l(r)}(i) = {\rm Round}\left[\left(\frac{1 \pm P^{\rm true}S_{\rm eff}}{2}\right)N_0(i)\,\frac{\varepsilon_{\rm 2CD}}{S^2_{\rm eff}}\right], \qquad (35)$$

where 'Round' indicates the approximation to the nearest integer value.

(c) We then used $N^0_{\rm l}(i)$ and $N^0_{\rm r}(i)$ as the two mean values of two Poissonians, and then *randomly* extracted two values, $N_{\rm l}(i)$ and $N_{\rm r}(i)$. This is done to resemble the Poissonian behaviour of the detectors.

(d) The polarization actually detected is thus calculated as

$$P^{\rm det}(i) = \frac{N_{\rm l}(i) - N_{\rm r}(i)}{N_{\rm l}(i) + N_{\rm r}(i)}\,\frac{1}{S_{\rm eff}}. \qquad (36)$$

(iv) With the array $P^{\rm det}(i = 1 : n_{\rm p}^{\rm max})$ of the detected polarization, we calculated the 'experimental' polarization $P(n_{\rm p})$ as a function of the number of measurement steps as the average of $P^{\rm det}(i = 1 : n_{\rm p}^{\rm max})$ up to $n_{\rm p}$:

$$P(n_{\rm p}) = \frac{1}{n_{\rm p}}\sum_{i=1}^{n_{\rm p}} P^{\rm det}(i), \qquad n_{\rm p} = 1, \ldots, n_{\rm p}^{\rm max}. \qquad (37)$$

(v) Finally, we defined a variance $\Delta P(n_{\rm p})$ from the true value $P^{\rm true}$ as

$$\Delta P(n_{\rm p}) = \left\{\left[P(n_{\rm p}) - P^{\rm true}\right]^2\right\}^{1/2}, \qquad n_{\rm p} = 1, \ldots, n_{\rm p}^{\rm max}. \qquad (38)$$

Each of these simulations, however, is not sufficient to give a significant comparison with equations (20) and (33), because the former are expressed in the *statistical limit*, *i.e.* for an infinite number of experiments at *each value* of $n_{\rm p}$. Therefore, a loop repeating each simulation $n_{\rm sim}$ times was devised, and the resulting values for each $n_{\rm p}$ were averaged. If $n_{\rm sim}$ is large enough to be treatable in the statistical limit, the results can then be compared with equations (20) and (33).

For 1CD detectors the procedure was slightly different. We list below the main differences:

(i) Each iteration represents a single measurement of electron SP and thus requires two independent measurement steps. Thus the iteration index j no longer coincides with the number of measurement steps, i. The jth measurement is then simulated with two independent extractions [labelled as $N^0_A(j)$ and $N^0_B(j)$] over the photoemitted electron Gaussian probability distribution. The first extraction is used to calculate $N^0_{\uparrow}(j)$ as:

$$N^0_{\uparrow\downarrow}(j) = {\rm Round}\left[\left(\frac{1 + P^{\rm true}S_{\rm eff}}{2}\right)N^0_{A,(B)}(j)\;\frac{\varepsilon_{\rm 1CD}}{S^2_{\rm eff}}\right]. \qquad (39)$$

Analogous to the 2CD system, $N_{\uparrow}^{0}(j)$ and $N_{\downarrow}^{0}(j)$ are then used as centres of Poissonian distributions from which the measured values $N_{\uparrow}(j)$ and $N_{\downarrow}(j)$ are extracted. The polarization is then evaluated as:

$$P^{\rm det}(j) = \frac{N_{\uparrow}(j) - N_{\downarrow}(j)}{N_{\uparrow}(j) + N_{\downarrow}(j)} \frac{1}{S_{\rm eff}}, \tag{40}$$

and the variance is determined accordingly.

(ii) It must be stressed that for 1CD the use of the same number of measurement steps leads to half the number of measurements with respect to 2CD. Therefore, when average values, as in equations (37) and (38), have to be computed, the summation boundaries must be modified, so $P(n_{\rm m})$ and $\Delta P(n_{\rm m})$ after $n_{\rm m}$ measurements now read as

$$P(n_{\rm m}) = \frac{1}{n_{\rm m}} \sum_{j=1}^{n_{\rm m}} P^{\rm det}(j), \tag{41}$$

$$\Delta P(n_{\rm m}) = \left\{ \left[P(n_{\rm m}) - P^{\rm true} \right]^2 \right\}^{1/2}, \tag{42}$$

with $n_{\rm m} = 1, \ldots, n_{\rm p}^{\rm max}/2$.

In order to check the validity of the statistical analysis discussed in §5 and the necessary approximations, the values of the variance were also calculated by direct substitution of the parameters in equations (19) and (31). The results are plotted in Figs. 3 and 4. The difference between the curves obtained from equations (19) and (31) and equations (20) and (33) in Fig. 4 shows the effects of the approximations of large $n_{\rm p}$. The simulated data show a variance that is always smaller than the statistical estimate, in agreement with the fact that error analysis should give a safe (*i.e.* as tight as possible, but by excess) evaluation of the experimental uncertainty.

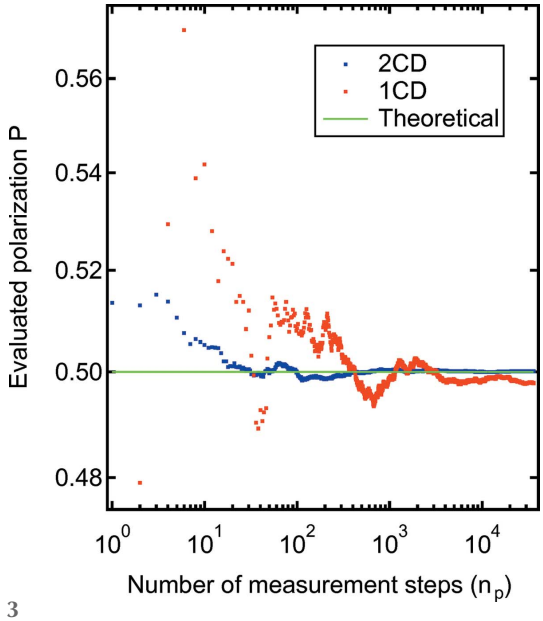

Figure 3
Result of measurement of a 50% polarization ($P^{\rm true} = 0.5$) with a 1CD (red) and 2CD (blue) as a function of the number of averaged measurement steps. Note that the curve of 1CD measurement sequence has only half of the points.

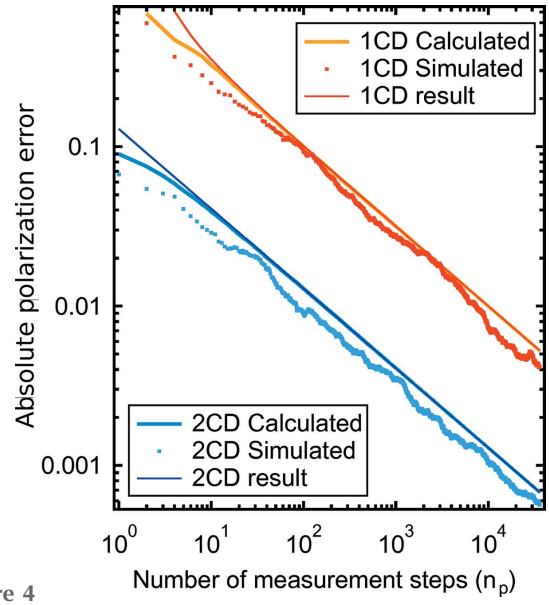

Figure 4
Results of a simulated run on a 1CD and 2CD detector. In this case, we used $n_{\rm p} = 36000$, corresponding to 1 h acquisition at 10 Hz, $\bar{N}_0 = 100000$, $\sigma_0 = 0.1$, $S_{\rm eff} = 0.36$ for 1CD, $\varepsilon_{\rm M} = 6 \times 10^{-4}$, $\varepsilon_{\rm V} = 1 \times 10^{-2}$, $N_{\rm sim} = 100$. The solid red and dark blue lines show the direct calculation form equations (19), (31), the light blue and orange lines show the results of our approximation for large $n_{\rm p}$, and the dots show the simulated measurements. Also here, the curve of 1CD measurement sequence has only half of the points.

7. Conclusions

We can therefore conclude that, relying on a solid statistical analysis, we demonstrated that in the pulsed source regime the FOM and effective Sherman function parameters are not comprehensive in describing the detector performance. Instead, the effect of the measurement routine and its interplay with the source time structure must be carefully accounted for.

Despite the lower FOM, indeed, parallel acquisition of asymmetry from two channels (or more) at once decouples the detector from the intensity variations of the source, allowing it to significantly outdo in terms of reduction of statistical error in SP measurement as a function of the averaged number of measurement steps. To prove this, we developed a rigorous description of statistical error for both kinds of detectors, obtaining simple and effective formulas that will be fundamental in the data analysis of this new technique. Finally, we verified such analysis with computational simulations that demonstrated the reliability of our conclusions.

We then mapped out the ranges (and consequently the state-of-the-art sources) in which each detector geometry performs best, individuating three regimes. In the medium–low intensity, small fluctuation regime typical of synchrotron and continuous sources, the high-FOM 1CDs are superior. In the high-brilliance, large shot-to-shot fluctuation pulsed regime characteristic of FELs or high-power solid-state laser sources, the 2CDs give the best statistics. Finally, in the regime of operation of HHG sources, with low photon flux, high shot-to-shot fluctuations, the performance of 1CDs and 2CDs is very close.

As time-resolved SP measurements are becoming ubiquitous in advanced spectroscopy of magnetic as well as non-magnetic strongly correlated systems, including spin-textured topological surfaces, and their dynamics needs to be studied, our analysis will be useful to guide the design and the data analysis of such experiments.

APPENDIX *A*
Calculation details

In this section, we expose the details of the calculation concerning the absolute error $\Delta N_{\rm pp}$ on the difference $N_0(i)\sigma_\uparrow - N_0(i+1)\sigma_\downarrow$.

Since $N_0(i)$ and $N_0(i+1)$ are two successive extractions of a normally distributed variable, it is possible to calculate $\Delta N_{\rm pp}$ as [for convenience of notation we set $N_0(i) = x$ and $N_0(i+1) = y$ and simplify the normalization factors]:

$$\begin{aligned}\Delta N_{\rm pp}^2 = &\left\{\int_0^\infty\int_0^\infty \left(x\sigma_\uparrow - y\sigma_\downarrow\right)^2 \exp\left[-(x-\bar N_0)^2/2\sigma_0^2\right]\right.\\ &\left.\times \exp\left[-(y-\bar N_0)^2/2\sigma_0^2\right]{\rm d}x\,{\rm d}y\right\}\\ &\Big/\left\{\int_0^\infty\int_0^\infty \exp\left[-(x-\bar N_0)^2/2\sigma_0^2\right]\right.\\ &\left.\times \exp\left[-(y-\bar N_0)^2/2\sigma_0^2\right]{\rm d}x\,{\rm d}y\right\}. \qquad (43)\end{aligned}$$

The lower integration limit can be extended to $-\infty$ because the central value $\bar N_0$ is positive and large. In this way we can use the known Gaussian integrals (Gradshteyn & Ryzhik, 2014) that give

$$\Delta N_{\rm pp}^2 = \bar N_0^2\left(\sigma_\uparrow - \sigma_\downarrow\right)^2 + \sigma_0^2\left(\sigma_\uparrow^2 + \sigma_\downarrow^2\right), \qquad (44)$$

hence,

$$\Delta N_{\rm pp}^2 = \bar N_0^2\left(\sigma_\uparrow^2 + \sigma_\downarrow^2\right)\left[\frac{\left(\sigma_\uparrow - \sigma_\downarrow\right)^2}{\sigma_\uparrow^2 + \sigma_\downarrow^2} + \gamma^2\right], \qquad (45)$$

where the aforementioned γ has been inserted. The first summand in the last term is small, and can be neglected, giving:

$$\begin{aligned}\Delta N_{\rm pp}^2 &= \bar N_0^2\left(\sigma_\uparrow^2 + \sigma_\downarrow^2\right)\gamma^2\\ &= \left(\bar N_\uparrow^2 + \bar N_\downarrow^2\right)\gamma^2\\ &\approx \frac{1}{2}\left(\bar N_\uparrow + \bar N_\downarrow\right)^2\gamma^2, \qquad (46)\end{aligned}$$

as $\bar N_\uparrow \simeq \bar N_\downarrow$. The result in equation (30) of the main text is thus justified.

APPENDIX *B*
Lightsources parameters

The detailed characteristics of the various sources considered in Fig. 2 of the main text are given in Table 2.

Acknowledgements

The authors acknowledge Dott. G. Panaccione for fruitful discussions. Funding from the PIK project (MIUR and

Table 2
Characteristics of the various sources considered in Fig. 2.

	Flux (photons s^{-1})	r.m.s. fluctuation (%)	Energy (eV)	Duration (ps)	Repetition rate (Hz)	Lens factor	Electron flux (e^- s^{-1})
A	10^9–10^{13}	0.1–0.5	Any† (20)	50	500×10^6	10^{-5}	10^3–10^7
B	2×10^{12}	0.15	21 (21)	–	–	10^{-5}	10^6
C	2×10^{15}	1	7 (7)	20	80×10^6	10^{-5}	10^7
D	–	0.25–5	500–4000 (1300)	–	–	10^{-3}	10^5–10^9
E	–	1	Any (20)	40	1×10^6	10^{-5}	2.5×10^3
E′	10^6	1	Any (20)	0.1	6×10^6	10^{-3}	10^2
E″	10^6	1	Any (20)	0.1	6×10^6	10^{-5}	10^0

† Can change in a very wide range, but photon flux values are for a UV spectroscopy beamline.

	Flux (photons $pulse^{-1}$)	r.m.s. fluctuation (%)	Energy (eV)	Duration (ps)	Repetition rate (Hz)	Lens factor	Electron flux (e^- $pulse^{-1}$)
F	8×10^{14}	5	6	0.1	1000	10^{-3}	10^8
G	10^{14}	25	10–60 (30)	0.1	10	10^{-3}	10^4–10^{10}
H	10^{13}	50	50–300 (100)	0.04–0.1	10	10^{-3}	10^4–10^9
I	10^{13}	60	30–300 (30)	0.05–0.2	10†	10^{-3}	10^4–10^9
J	10^8	25	10–90 (30)	0.3	20×10^3	10^{-3}	10^4
J′	10^8	25	10–90 (30)	0.3	20×10^3	10^{-5}	10^2
K	10^7	25	10–90 (30)	0.3	100×10^3	10^{-3}	10^3
K′	10^7	25	10–90 (30)	0.3	100×10^3	10^{-5}	10^1
L	10^6	26.6	10–90 (30)	0.3	3×10^3	10^{-3}	10^2
L′	10^6	26.6	10–90 (30)	0.3	3×10^3	10^{-5}	10^0

† FLASH delivers 10 Hz bursts. Within each burst the pulses are produced with repetition rates that go from 40 kHz to 1 MHz.

Sincrotrone Trieste) ULTRASPIN is acknowledged. This work has been partly supported by the NFFA-MIUR project (http://www.trieste.nffa.eu/), by IOM-CNR and by NOXSS PRIN (2012Z3N9R9) Project of MIUR, Italy.

References

Allaria, E., Appio, R., Badano, L., Barletta, W. A., Bassanese, S., Biedron, S. G., Borga, A., Busetto, E., Castronovo, D., Cinquegrana, P., Cleva, S., Cocco, D., Cornacchia, M., Craievich, P., Cudin, I., D'Auria, G., Dal Forno, M., Danailov, M. B., De Monte, R., De Ninno, G., Delgiusto, P., Demidovich, A., Di Mitri, S., Diviacco, B., Fabris, A., Fabris, R., Fawley, W., Ferianis, M., Ferrari, E., Ferry, S., Froehlich, L., Furlan, P., Gaio, G., Gelmetti, F., Giannessi, L., Giannini, M., Gobessi, R., Ivanov, R., Karantzoulis, E., Lonza, M., Lutman, A., Mahieu, B., Milloch, M., Milton, S. V., Musardo, M., Nikolov, I., Noe, S., Parmigiani, F., Penco, G., Petronio, M., Pivetta, L., Predonzani, M., Rossi, F., Rumiz, L., Salom, A., Scafuri, C., Serpico, C., Sigalotti, P., Spampinati, S., Spezzani, C., Svandrlik, M., Svetina, C., Tazzari, S., Trovo, M., Umer, R., Vascotto, A., Veronese, M., Visintini, R., Zaccaria, M., Zangrando, D. & Zangrando, M. (2012). *Nat. Photon.* **6**, 699–704.

Allaria, E., Castronovo, D., Cinquegrana, P., Craievich, P., Dal Forno, M., Danailov, M. B., D'Auria, G., Demidovich, A., De Ninno, G., Di Mitri, S., Diviacco, B., Fawley, W. M., Ferianis, M., Ferrari, E., Froehlich, L., Gaio, G., Gauthier, D., Giannessi, L., Ivanov, R., Mahieu, B., Mahne, N., Nikolov, I., Parmigiani, F., Penco, G., Raimondi, L., Scafuri, C., Serpico, C., Sigalotti, P., Spampinati, S., Spezzani, C., Svandrlik, M., Svetina, C., Trovo, M., Veronese, M., Zangrando, D. & Zangrando, M. (2013). *Nature Photon*, **7**, 913–918.

Amann, J., Berg, W., Blank, V., Decker, F.-J., Ding, Y., Emma, P., Feng, Y., Frisch, J., Fritz, D., Hastings, J., Huang, Z., Krzywinski, J., Lindberg, R., Loos, H., Lutman, A., Nuhn, H.-D., Ratner, D., Rzepiela, J., Shu, D., Shvyd'ko, Yu., Spampinati, S., Stoupin, S., Terentyev, S., Trakhtenberg, E., Walz, D., Welch, J., Wu, J., Zholents, A. & Zhu, D. (2012). *Nat. Photon.* **6**, 693–698.

Ayvazyan, V., Baboi, N., Bähr, J., Balandin, V., Beutner, B., Brandt, A., Bohnet, I., Bolzmann, A., Brinkmann, R., Brovko, O. I., Carneiro, J. P., Casalbuoni, S., Castellano, M., Castro, P., Catani, L., Chiadroni, E., Choroba, S., Cianchi, A., Delsim-Hashemi, H., Di Pirro, G., Dohlus, M., Düsterer, S., Edwards, H. T., Faatz, B., Fateev, A. A., Feldhaus, J., Flöttmann, K., Frisch, J., Fröhlich, L., Garvey, T., Gensch, U., Golubeva, N., Grabosch, H.-J., Grigoryan, B., Grimm, O., Hahn, U., Han, J. H., Hartrott, M. V., Honkavaara, K., Hüning, M., Ischebeck, R., Jaeschke, E., Jablonka, M., Kammering, R., Katalev, V., Keitel, B., Khodyachykh, S., Kim, Y., Kocharyan, V., Körfer, M., Kollewe, M., Kostin, D., Krämer, D., Krassilnikov, M., Kube, G., Lilje, L., Limberg, T., Lipka, D., Löhl, F., Luong, M., Magne, C., Menzel, J., Michelato, P., Miltchev, V., Minty, M., Möller, W. D., Monaco, L., Müller, W., Nagl, M., Napoly, O., Nicolosi, P., Nölle, D., Nuñez, T., Oppelt, A., Pagani, C., Paparella, R., Petersen, B., Petrosyan, B., Pflüger, J., Piot, P., Plönjes, E., Poletto, L., Proch, D., Pugachov, D., Rehlich, K., Richter, D., Riemann, S., Ross, M., Rossbach, J., Sachwitz, M., Saldin, E. L., Sandner, W., Schlarb, H., Schmidt, B., Schmitz, M., Schmüser, P., Schneider, J. R., Schneidmiller, E. A., Schreiber, H.-J., Schreiber, S., Shabunov, A. V., Sertore, D., Setzer, S., Simrock, S., Sombrowski, E., Staykov, L., Steffen, B., Stephan, F., Stulle, F., Sytchev, K. P., Thom, H., Tiedtke, K., Tischer, M., Treusch, R., Trines, D., Tsakov, I., Vardanyan, A., Wanzenberg, R., Weiland, T., Weise, H., Wendt, M., Will, I., Winter, A., Wittenburg, K., Yurkov, M. V., Zagorodnov, I., Zambolin, P. & Zapfe, K. (2006). *Eur. Phys. J. D*, **37**, 297–303.

Bergeard, N., Silly, M. G., Krizmancic, D., Chauvet, C., Guzzo, M., Ricaud, J. P., Izquierdo, M., Stebel, L., Pittana, P., Sergo, R., Cautero, G., Dufour, G., Rochet, F. & Sirotti, F. (2011). *J. Synchrotron Rad.* **18**, 245–250.

Bertacco, R. & Ciccacci, F. (1999). *Surf. Sci.* **419**, 265–271.

Bertacco, R., Merano, M. & Ciccacci, F. (1998). *Appl. Phys. Lett.* **72**, 2050–2052.

Bigi, C. (2016). Master's thesis, Università degli studi di Milano, Italy.

Burnett, G. C., Monroe, T. J. & Dunning, F. B. (1994). *Rev. Sci. Instrum.* **65**, 1893–1896.

Das, P. K., Di Sante, D., Vobornik, I., Fujii, J., Okuda, T., Bruyer, E., Gyenis, A., Feldman, B. E., Tao, J., Ciancio, R., Rossi, G., Ali, M. N., Picozzi, S., Yadzani, A., Panaccione, G. & Cava, R. J. (2016). *Nat. Commun.* **7**, 10847.

Dell'Angela, M., Anniyev, T., Beye, M., Coffee, R., Föhlisch, A., Gladh, J., Kaya, S., Katayama, T., Krupin, O., Nilsson, A., Nordlund, D., Schlotter, W. F., Sellberg, J. A., Sorgenfrei, F., Turner, J. J., Öström, H., Ogasawara, H., Wolf, M. & Wurth, W. (2015). *Struct. Dyn.* **2**, 025101.

Dil, J. H. (2009). *J. Phys. Condens. Matter*, **21**, 403001.

Fognini, A., Salvatella, G., Michlmayr, T., Wetli, C., Ramsperger, U., Bähler, T., Sorgenfrei, F., Beye, M., Eschenlohr, A., Pontius, N., Stamm, C., Hieke, F., Dell'Angela, M., de Jong, S., Kukreja, R., Gerasimova, N., Rybnikov, V., Redlin, H., Raabe, J., Föhlisch, A., Dürr, H. A., Wurth, W., Pescia, D., Vaterlaus, A. & Acremann, Y. (2014). *New J. Phys.* **16**, 043031.

Galayda, J. N., Arthur, J., Ratner, D. F. & White, W. E. (2010). *J. Opt. Soc. Am. B*, **27**, B106–B118.

Gay, T. J. & Dunning, F. B. (1992). *Rev. Sci. Instrum.* **63**, 1635–1651.

Gay, T. J., Khakoo, M., Brand, J., Furst, J., Meyer, W., Wijayaratna, W. & Dunning, F. (1992). *Rev. Sci. Instrum.* **63**, 114–130.

Getzlaff, M., Heidemann, B., Bansmann, J., Westphal, C. & Schönhense, G. (1998). *Rev. Sci. Instrum.* **69**, 3913–3923.

Gradshteyn, I. S. & Ryzhik, I. M. (2014). *Table of Integrals, Series, and Products.* Elsevier Science.

Graf, J., Jozwiak, C., Schmid, A. K., Hussain, Z. & Lanzara, A. (2005). *Phys. Rev. B*, **71**, 144429.

Hara, T., Togawa, K. & Tanaka, H. (2012). *Proceedings of the 34th International Free-Electron Laser Conference (FEL2012)*, 26–31 August 2012, Nara, Japan, pp. 5–8. JACoW.

Hellmann, S., Rossnagel, K., Marczynski-Bühlow, M. & Kipp, L. (2009). *Phys. Rev. B*, **79**, 035402.

Hellmann, S., Sohrt, C., Beye, M., Rohwer, T., Sorgenfrei, F., Marczynski-Bühlow, M., Kalläne, M., Redlin, H., Hennies, F., Bauer, M., Föhlisch, A., Kipp, L., Wurth, W. & Rossnagel, K. (2012). *New J. Phys.* **14**, 013062.

Hoesch, M., Greber, T., Petrov, V., Muntwiler, M., Hengsberger, M., Auwärter, W. & Osterwalder, J. (2002). *J. Electron Spectrosc. Relat. Phenom.* **124**, 263–279.

Holldack, K., Bahrdt, J., Balzer, A., Bovensiepen, U., Brzhezinskaya, M., Erko, A., Eschenlohr, A., Follath, R., Firsov, A., Frentrup, W., Le Guyader, L., Kachel, T., Kuske, P., Mitzner, R., Müller, R., Pontius, N., Quast, T., Radu, I., Schmidt, J.-S., Schüßler-Langeheine, C., Sperling, M., Stamm, C., Trabant, C. & Föhlisch, A. (2014). *J. Synchrotron Rad.* **21**, 1090–1104.

Kessler, J. (1985). *Polarized Electrons.* Berlin/Heidelberg: Springer-Verlag.

Kirschner, J., Giebels, F., Gollisch, H. & Feder, R. (2013). *Phys. Rev. B*, **88**, 125419.

Kutnyakhov, D., Lushchyk, P., Fognini, A., Perriard, D., Kolbe, M., Medjanik, K., Fedchenko, E., Nepijko, S., Elmers, H., Salvatella, G., Stieger, C., Gort, R., Bähler, T., Michlmayer, T., Acremann, Y., Vaterlaus, A., Giebels, F., Gollisch, H., Feder, R., Tusche, C., Krasyuk, A., Kirschner, J. & Schönhense, G. (2013*a*). *Ultramicroscopy*, **130**, 63–69.

Leitner, T., Sorokin, A. A., Gaudin, J., Kaser, H., Kroth, U., Tiedtke, K., Richter, M. & Wernet, P. (2011). *New J. Phys.* **13**, 093003.

Lorek, E., Larsen, E. W., Heyl, C. M., Carlström, S., Paleček, D., Zigmantas, D. & Mauritsson, J. (2014). *Rev. Sci. Instrum.* **85**, 123106.

Mott, N. F. (1929). *Proc. R. Soc. A*, **124**, 425–442.

Mott, N. F. (1932). *Proc. R. Soc. A*, **135**, 429–458.

Okuda, T., Miyamaoto, K., Miyahara, H., Kuroda, K., Kimura, A., Namatame, H. & Taniguchi, M. (2011). *Rev. Sci. Instrum.* **82**, 103302.
Petrov, V. N., Grebenshikov, V. V., Andronov, A. N., Gabdullin, P. G. & Maslevtcov, A. V. (2007). *Rev. Sci. Instrum.* **78**, 025102.
Petrov, V. N., Grebenshikov, V. V., Grachev, B. D. & Kamochkin, A. S. (2003). *Rev. Sci. Instrum.* **74**, 1278–1281.
Petrov, V. N. & Kamochkin, A. S. (2004). *Rev. Sci. Instrum.* **75**, 1274–1279.
Pincelli, T., Petrov, V. N., Brajnik, G., Ciprian, R., Lollobrigida, V., Torelli, P., Krizmancic, D., Salvador, F., Luisa, A. D., Sergo, R., Gubertini, A., Cautero, G., Carrato, S., Rossi, G. & Panaccione, G. (2016). *Rev. Sci. Instrum.* **87**, 4943255.
Schönhense, G., Medjanik, K. & Elmers, H. (2015). *J. Electron Spectrosc. Relat. Phenom.* **200**, 94–118.
Sherman, N. (1956). *Phys. Rev.* **103**, 1601–1607.
Shimojima, T., Okazaki, K. & Shin, S. (2015). *J. Phys. Soc. Jpn*, **84**, 072001.
Shull, C. G., Chase, C. T. & Myers, F. E. (1943). *Phys. Rev.* **63**, 29–37.
Strocov, V. N., Petrov, V. N. & Dil, J. H. (2015). *J. Synchrotron Rad.* **22**, 708–716.
Suzuki, R., Sakano, M., Zhang, Y., Akashi, R., Morikawa, D., Harasawa, A., Yaji, K., Kuroda, K., Miyamoto, K., Okuda, T., Ishizaka, K., Arita, R. & Iwasa, Y. (2014). *Nat. Nanotechnol.* **9**, 611–617.
Tusche, C., Ellguth, M., Krasyuk, A., Winkelmann, A., Kutnyakhov, D., Lushchyk, P., Medjanik, K., Schönhense, G. & Kirschner, J. (2013). *Ultramicroscopy*, **130**, 70–76.
Verna, A., Greco, G., Lollobrigida, V., Offi, F. & Stefani, G. (2016). *J. Electron Spectrosc. Relat. Phenom.* **209**, 14–25.
Yu, D., Math, C., Meier, M., Escher, M., Rangelov, G. & Donath, M. (2007). *Surf. Sci.* **601**, 5803–5808.